Remote Sensing of Environment 308 (2024) 114194

Contents lists available at ScienceDirect

Remote Sensing of Environment

journal homepage: www.elsevier.com/locate/rse

Unmixing-based forest recovery indicators for predicting long-term recovery success

Lisa Mandl [a,b,c,*], Alba Viana-Soto [a], Rupert Seidl [b,c], Ana Stritih [b,c], Cornelius Senf [a]

[a] Earth Observation for Ecosystem Management, School of Life Sciences, Technical University of Munich, Freising, Germany
[b] Ecosystem Dynamics and Forest Management in Mountain Landscapes, School of Life Sciences, Technical University of Munich, Freising, Germany
[c] Berchtesgaden National Park, Research and Monitoring, Berchtesgaden, Germany

ARTICLE INFO

Edited by Marie Weiss

Keywords:
Post-disturbance forest recovery
Synthetic spectral unmixing
Fractional cover mapping
Landsat
Sentinel-2
Alps

ABSTRACT

Recovery from forest disturbances is a pivotal metric of forest resilience. Forests globally are facing unprecedented levels of both natural and anthropogenic disturbances, yet our understanding of their recovery from these disturbances remains incomplete. Remote sensing is an effective tool for understanding post-disturbance recovery, but existing approaches largely rely on spectral recovery indicators that are difficult to interpret and require long time series after disturbance, which limits their applicability to recent disturbance pulses. We here introduce a novel, ecologically informed set of recovery indicators based on fractional cover maps derived from spectral unmixing analysis of Landsat and Sentinel-2 time series. We estimated annual pre- and post-disturbance tree cover and bare ground fractions over the eastern Alps (~130,000 km^2) for the period from 1990 to 2021. From these fraction time series, we derived recovery intervals defined as the time it takes to reach a pre-defined tree cover threshold after disturbance, referred to as canopy recovery. We found mean recovery intervals between 5.5 and 13.4 years, depending on recovery threshold and disturbance severity. Comparing our results to traditional remote sensing-based approaches of mapping forest recovery, we found that spectral unmixing-based recovery indicators give considerably more realistic recovery intervals than approaches based on spectral indices because they effectively distinguish tree regeneration from other post-disturbance vegetation (e.g., shrubs, grasses). Finally, we were able to accurately predict the long-term forest recovery success based on the information available only three years after disturbance, which underlines the high importance of a short window of reorganization post-disturbance, and highlights the utility of remote sensing to inform post-disturbance forest management (e.g., in identifying areas in need of tree planting). Our study thus provides an important step ahead in the remote sensing-based monitoring of forest recovery and resilience, which is urgently needed in a time of rapid forest change.

1. Introduction

Forests in Europe have experienced an increase in disturbances in the past four decades (Senf et al., 2018) which has sparked interest in assessing post-disturbance forest recovery (Seidl and Turner, 2022). Forest recovery is, however, a broad term, and it can be measured in different dimensions (e.g., structure, composition, or function). A key dimension of structural forest recovery is canopy cover, which can be defined as the reestablishment of a closed tree canopy (Grantham et al., 2020). Post-disturbance canopy recovery is a pivotal process for assessing forest resilience (Ingrisch and Bahn, 2018; Stritih et al., 2023) because it reflects the potential of a forest to regain the capacity for important ecosystem functions and services (Trumbore et al., 2015). Such functions and services include, among other, protection from natural hazards (Sebald et al., 2019) or water purification (Jung et al., 2021). A European-wide study by Senf and Seidl (2022) showed that most forests return to a closed canopy state within 30 years after disturbance. However, soil loss and competition from graminoids can impede the establishments of seeds and the growth of saplings (Zehetgruber et al., 2017). Increasing climate extremes pose additional challenges during the initial recovery phases (Beloiu et al., 2022; Hérault and Piponiot, 2018; Stevens-Rumann et al., 2022), which likely will become more significant in the future. There is thus growing uncertainty regarding the successful recovery of forests to closed canopy conditions

* Corresponding author at: Earth Observation for Ecosystem Management, School of Life Sciences, Technical University of Munich, Freising, Germany.
E-mail address: lisa.mandl@tum.de (L. Mandl).

https://doi.org/10.1016/j.rse.2024.114194
Received 5 February 2024; Received in revised form 29 April 2024; Accepted 1 May 2024
Available online 9 May 2024
0034-4257/© 2024 The Authors. Published by Elsevier Inc. This is an open access article under the CC BY license (http://creativecommons.org/licenses/by/4.0/).

after disturbances (McDowell et al., 2020; Seidl and Turner, 2022), which highlights the need for a comprehensive monitoring of forest recovery across space and time.

A variety of studies have assessed post-disturbance recovery using field data on post-disturbance tree densities (Strickland et al., 2024), including a recent large-scale study across Europe (Cerioni et al., 2024). While those studies give valuable insights into the establishment of trees after disturbance, they often only present a snapshot in time and thus do not fully capture the temporal dynamics of forest recovery to closed canopy conditions. Field-based approaches also rarely allow for spatially explicit analyses of recovery, because field data are labor-intensive to collect, and most datasets thus only represent a limited sample of disturbed sites. Remote sensing has been suggested as a complementary tool for studying post-disturbance recovery (Frolking et al., 2009), overcoming some of the limitations of field-based approaches. Special emphasis has been given to long time series of multispectral observations, now spanning over 50 years with regular (theoretically 8–16 days) multispectral observations (Wulder et al., 2022). The long data history has led to numerous studies investigating post-disturbance forest recovery using spectral indices: In earlier studies, the Normalized Difference Vegetation Index (NDVI) was commonly used for post-disturbance recovery assessments, particularly after events like fires (Gitas et al., 2012; Solans Vila and Barbosa, 2010; Veraverbeke et al., 2013). However, the quick saturation of NDVI after disturbances, attributed to early successional vegetation, limits its application in capturing and distinguishing changes in post-disturbance vegetation structure (Buma, 2012). To address this problem, it was suggested to adopt alternative indices based on the short-wave infrared region, such as the Normalized Burn Ratio (NBR), which offers a higher sensitivity to post-disturbance structural changes (Pickell et al., 2016). The NBR has consequently been operational in assessing forest recovery across a wide range of forest ecosystem, from boreal to Mediterranean biomes (Chirici et al., 2020; Frazier et al., 2018; Hermosilla et al., 2019; Nikinmaa et al., 2020; White et al., 2022; White et al., 2018; White et al., 2017).

What all approaches for assessing recovery based on spectral indices have in common is the need to define a recovery threshold. Most studies define this threshold as 80% of the pre-disturbance average index value, which was found to correspond well to LiDAR-derived measures of recovery in a case study in Finland (White et al., 2018). Yet, an 80% threshold might not always signify structural or compositional recovery, as highlighted recently by White et al., 2023, and might not correspond to established definitions of forest cover. Other studies have used multiple indices to gain a more comprehensive understanding of recovery processes (Hislop et al., 2018; Liu et al., 2023; Pickell et al., 2016; Smith-Tripp et al., 2024), but defining a reference state for multiple spectral indices is even more challenging, as different indices contain different information on the recovery process (Pickell et al., 2016). Another important drawback of spectral indices is their inability to distinguish between different vegetation types and consequently their limitation in assessing which factors drive the observed increase in the respective index. It thus remains unclear whether spectral recovery does indeed signify recovery of the tree canopy, or just an increase in vegetation density after disturbance. To overcome these limitations, it has been suggested to convert spectral recovery trajectories into trajectories of tree cover using either regression models (Senf et al., 2019; Senf and Seidl, 2022) or spectral unmixing (Senf et al., 2020). Doing so allows for defining distinct recovery thresholds based on a physically meaningful unit (e.g., 80% of pre-disturbance canopy cover) or for defining fixed thresholds based on existing definitions (e.g., $>$ 40% tree cover as defined by the FAO as closed forest).

Estimating if and how quickly a forest recovers its canopy after disturbance requires decadal time series, as most forests will take years to decades to close their canopy (Senf and Seidl, 2022). This constraint makes it challenging to predict recovery for recently disturbed sites, which have not yet closed their canopy. The need for long time series also makes it challenging to assess potential changes in recovery over time, which would be an important early warning signal for eroding forest resilience (Scheffer et al., 2015). Given those limitations, a key question is whether the long-term recovery of a forest can be predicted already from early post-disturbance site characteristics. This question follows the notion that forest recovery trajectories are, to a large degree, determined in a short reorganization window after disturbance (Seidl and Turner, 2022) that might be captured by remote sensing. For example, high disturbance severities and high shares of bare ground shortly after disturbance might indicate a severe impact on local soil conditions (i.e., through heavy machinery used in post-disturbance salvage logging) and thus reduced seed establishment. It likewise might indicate a reduced seed availability (i.e., local loss of all mature trees) and increased light availability, which can hinder forest recovery by favouring the dominance of competing vegetation such as graminoids (Kleinman et al., 2019; Mantero et al., 2023). Conversely, low disturbance severities and low bare ground fractions shortly after disturbance might indicate the presence of remaining mature trees, advanced tree regeneration and shrubs, which are associated with a faster recovery due to higher seed availability (Ibáñez et al., 2019) and more favourable microclimate conditions (Alfaro-Sánchez et al., 2015; Marcolin et al., 2019). To quantify early post-disturbance conditions as a window into the future recovery trajectory of a forest, we propose the use of spectral unmixing to derive early post-disturbance fractions of bare ground (Schug et al., 2020). We hypothesize that early post-disturbance bare ground fractions, in combination with disturbance characteristics (i.e., disturbance severity, pre-disturbance canopy cover), can provide valuable insights into the long-term recovery probability of a pixel.

Here, our aim is to develop a novel, ecologically informed set of remote sensing-based recovery indicators using spectral unmixing. We address our overall aim by focusing on two specific objectives: (a) compare recovery intervals derived from spectral unmixing and based on physical units of tree cover to existing recovery indicators based on spectral indices across variable disturbance characteristics; and (b) test whether post-disturbance bare ground fractions and disturbance characteristics can be used to predict long-term recovery probabilities. We approach all objectives for a study system located in the Eastern Alps of Central Europe, covering 130,000 km^2 and a wide range of different forest types and disturbance regimes.

2. Study system

Our study system encompasses the entire eastern Alps in Europe (Fig. 1), stretching from Munich in the north to Verona in the south (48.5° N to 45.5° N) and from Zurich in the west to Vienna in the east (9° E to 16.5° E), with approximately 130,000 km^2 of land surface, of which ~70.000 km^2 are forests (Senf and Seidl, 2021). The study system has a distinctive geographical and ecological profile, with strong elevational gradients from lowlands at around sea level to altitudes of 4048 m a.s.l. (Piz Bernina), with the average potential tree line being between 2000 and 2350 m a.s.l (Pecher et al., 2011). The climate of the eastern Alps is influenced by their geographical location between the temperate and Mediterranean biomes and by their strong topographical gradients, from relatively mild temperatures in the colline and montane elevation zone to cold conditions at higher elevations. Mean annual temperature is −0.7 °C for the climate period 1991–2020 (Nigrelli and Chiarle, 2023) and mean annual precipitation is around 1100 mm (Frei and Schär, 1998), yet both vary substantially with elevation. The Alps showcase a remarkable diversity of vegetation and forest types, with deciduous broadleaf forests, primarily dominated by European beech (*Fagus sylvatica* L.), being the most prevalent potential natural vegetation type (Bohn et al., 2000). However, the composition of these forests has been significantly altered due to historical land use practices, with forest management favouring Norway spruce (*Picea abies* (L.) Karst.) – naturally occurring in montane and subalpine forests – even at lower elevations. At higher elevations, broadleaved species are widely replaced by coniferous species, including Norway spruce, Silver fir (*Abies alba*

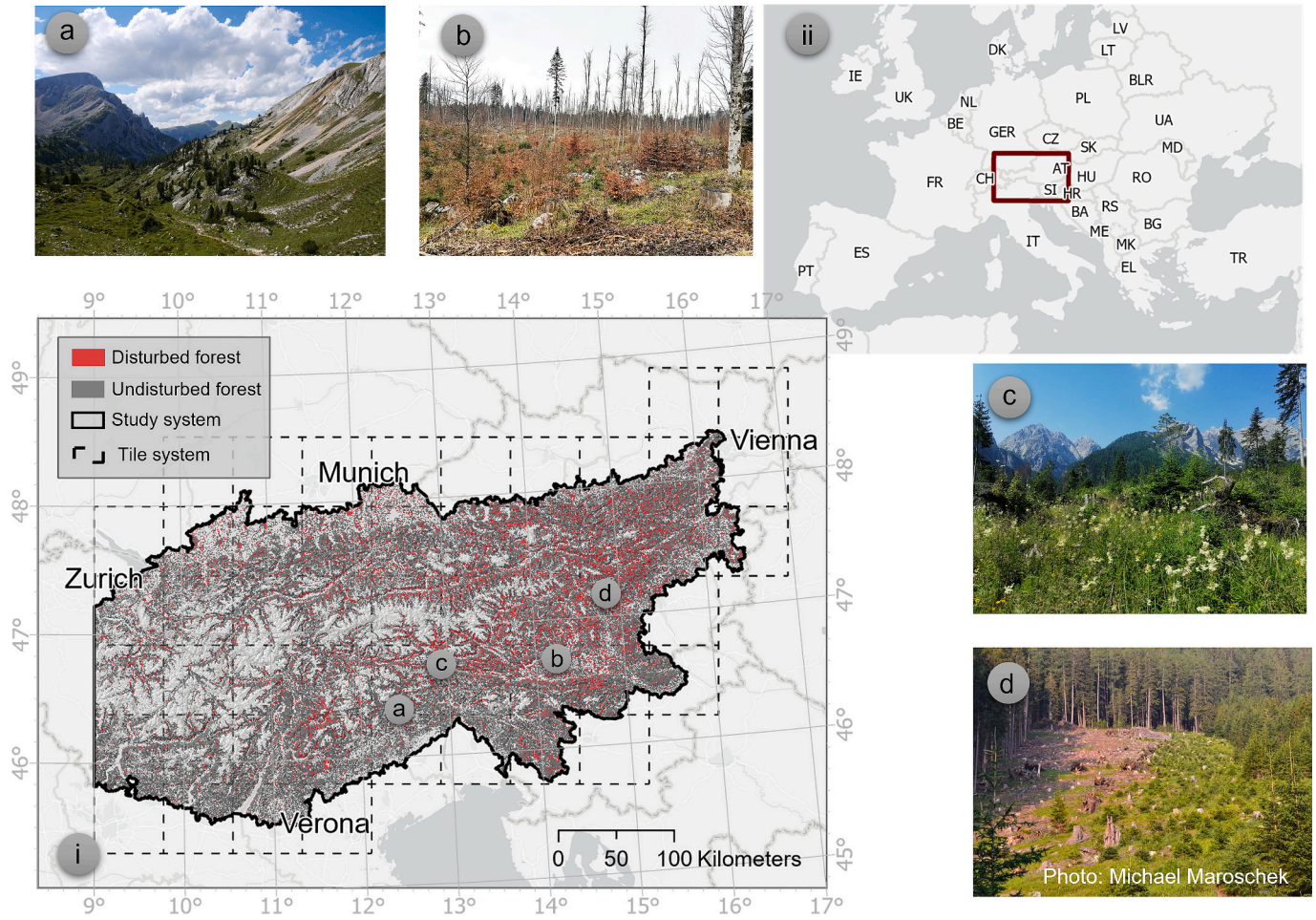

Fig. 1. The study system of the Eastern Alps (i) and its location in Central Europe (ii). (a) represents a typical, sub-alpine non-disturbed landscape configuration in the Alps with trees, bare ground and alpine grassland. (b), (c) and (d) show different post-disturbance states with a mixture of dead trees, remaining trees and shrubland, mainly grassland, and grassland with planted seedlings and a relatively high bare ground share.

Mill.), European larch (*Larix decidua* L.), Swiss stone pine (*Pinus cembra* L.) and mountain pine (*Pinus mugo* Turra). Additionally, the region hosts a variety of shrubs, including green alder (*Alnus viridis* (Ehrh.) K. Koch), contributing to the overall ecological complexity of the area (Rüetschi et al., 2021). Historical land-use practices, such as the expansion of pastures for grazing, anthropogenic fires, and intensive ungulate browsing have significantly shaped forest and disturbance dynamics in the European Alps. These practices have had long-lasting effects that continue to strongly impact disturbance regimes in the area (Bebi et al., 2017). In the last decades, the European Alps have experienced an increasing frequency of natural disturbances likely related to increasing climate extremes and past land use practices (Sebald et al., 2021; Senf et al., 2021; Stritih et al., 2021b), with storms, bark beetle outbreaks, avalanches and wildfires being the most prevalent natural disturbance agents (Bebi et al., 2017). While the size of natural disturbances in the Alps is generally small (Maroschek et al., 2023), salvage logging and human management have altered disturbance regimes in the region: Based on a recent disturbance map derived from Landsat data (see details in Senf and Seidl, 2021) we identified a total of 1.76 10^6 patches in our study system with a median patch size of 0.36 ha, summing to an average disturbed area of 320 km^2 per year, with a standard deviation of 150 km^2. The most disturbances were identified in the years 2003, 2007 and 2019, following three major storm events (Foehn storm Uschi in 2003, storm Kyrill in 2007 and storm Vaia in 2018) with subsequent bark beetle outbreaks. All following analysis will focus on these disturbed areas.

3. Data & methods

3.1. Building a consistent data cube from Landsat 4–8 and Sentinel-2

We retrieved all available Landsat 4–8 and Sentinel-2 A/B images between 1990 and 2021 with a maximum cloud cover of 60% from the Google cloud storage (https://cloud.google.com/storage/docs/public-datasets/). We incorporated all available images, thus not focusing on specific seasons. This resulted in a total of 7701 Landsat images and 13,960 Sentinel-2 images. Both Landsat and Sentinel-2 data were processed to Level 2 Analysis Ready Data (ARD) using the Framework for Operational Radiometric Correction for Environmental Monitoring (FORCE version 3.7.10, (Frantz, 2019)), which stores the final ARD in non-overlapping 60 km × 60 km tiles. The 10 and 20 m bands of the Sentinel-2 Multispectral Imager (MSI) were resampled to 30 m to match the spatial resolution of Landsat. Pre-processing to Level 2 consisted of radiometric processing as well as correcting atmospheric, topographic and bidirectional effects (Frantz et al., 2016; Roy et al., 2016; Zhu and Woodcock, 2012). For the atmospheric and topographic correction, we used the Copernicus DEM with 25 m resolution (EU-DEM v1.1 2016) and a pre-compiled water vapor database (Frantz, 2019). We also masked clouds, cloud shadows and snow using an adapted version of the Fmask algorithm (Frantz et al., 2018; Zhu and Woodcock, 2014). To fix geometric misalignment between Landsat and Sentinel-2 data, we performed a co-registration by employing Landsat level 2 NIR composites as base images using the LSReg algorithm (Frantz, 2019; Rufin et al., 2021;

Yan et al., 2016).

The Level 2 processed Landsat and Sentinel-2 data were converted to a collection of spectral-temporal metrics, which represent annual statistical aggregations of the spectral characteristics at the pixel level (Frantz, 2019). This step was necessary to build a consistent annual time series of predictors to be used in the spectral unmixing described below, accounting for varying observations densities over time. We employed the 25th, 50th, and 75th quantiles of annual Landsat and Sentinel-2 reflectance values and the 90th percentile and standard deviation of common spectral indices (Normalized Difference Vegetation Index (NDVI; Kriegler et al., 1969), Enhanced Vegetation Index (EVI; Liu and Huete, 1995), Normalized Burn Ratio (NBR; García and Caselles, 1991), Normalized Difference Moisture Index (NDMI; Buschmann and Nagel, 1993), Soil-Adjusted Vegetation Index (SAVI; Huete, 1988), Normalized Difference Water Index (NDWI; Gao, 1996), Normalized Difference Snow Index (NDSI; Riggs et al., 1994)). This combination was also successfully applied in previous synthetic spectral unmixing studies (Haberl et al., 2021; Okujeni et al., 2021; Schug et al., 2020; Viana-Soto et al., 2022).

3.2. Spectral unmixing

We applied spectral unmixing analysis (Cooper et al., 2020; Okujeni et al., 2018) to convert the spectral-temporal metrics (STMs) described above into annual fractions of land cover. Spectral unmixing is a well-suited tool for describing disturbance and recovery trajectories (Senf et al., 2020; Viana-Soto et al., 2022), because disturbed sites will be covered by a mix of remnant trees, shrubs, grasses and soil. Spectral unmixing enables to decompose a post-disturbance pixel into fractions of each of these cover type. Spectral unmixing, as implemented in this study and based on Okujeni et al., 2013 and Okujeni et al., 2017, involves several key steps. Initially, endmembers, serving as pure spectral signatures of various land cover classes, are used as reference spectra. Following this, spectral-temporal metrics (STMs) are synthetically combined at the locations of endmembers into various mixing proportions. This generates a training dataset that represents diverse combinations of land cover classes. Subsequently, Support Vector Regression (SVR) is applied to this training dataset to predict fractional land cover at annual scale. Each step will be described in more detail in the following, for a visual representation of the entire workflow, please see Fig. S1.

We developed a multi-year endmember library consisting of pure and temporally stable pixels for the target classes *tree cover*, *bare ground,* and *shrubs/grassland*, representing the major post-disturbance land cover types (see also Table 1). To pre-select candidate pixels for the endmember library, we utilized the LUCAS (Land Use/Cover Area frame Statistical Survey) database, which provides harmonized in-situ data on land cover and land use from 2006 to 2018. LUCAS aims at gathering comprehensive and standardized data on land use and land cover across EU member states. The database employs a stratified random sampling design, with trained field surveyors conducting on-site measurements to evaluate various characteristics including local land cover (d'Andrimont et al., 2020). Additionally, some survey plots include photographs, which further aided in the pre-selection process for the endmember library compiled here. Visual examples of endmembers with high-resolution aerial imagery and spectral profiles can be found in the Fig. S2. To ensure the greatest possible purity in our endmembers (i.e. the absence of other land cover classes in a pixel), we only included points with a cover value of >75% in the pre-selection. In addition, we integrated a forest mask developed by Senf and Seidl, 2021 to ensure that tree cover endmembers are not located at forest edges, and leveraged Google Earth imagery to corroborate the selection of our candidate endmembers. To validate the pre-selection, we conducted an analysis of NDVI values over time. Pixels were considered suitable endmember candidates if their NDVI values exhibited minimal fluctuations, indicating temporal stability (see Fig. S3). As an additional step, we performed a feature space analysis to refine our selection process further (see Fig. S4). The outcome of this pre-selection yielded a total of 39 pixels for tree cover, 87 for shrubs/grassland, and 44 for bare ground. For their geographic distribution see Fig. S5, for endmember examples and their spectral profiles, see Figs. S2 and S6.

Table 1
Endmember classes and corresponding LUCAS level 3 land cover codes, classes and the number of points per class used for creating synthetic training data.

Endmember class	Code	Land cover class (level 3)	Number of points
Tree cover	C10	Broadleaved woodland	16
	C20	Coniferous woodland	23
Shrubs/ grassland	D20	Shrubland without tree cover	11
	E20	Grassland without tree/shrub cover	66
Bare ground	F10	Rock and stones	24
	F30	Lichen and moss	9
	F40	Other bare soil (containing bare arable land, temporarily unstocked areas within forests with bare soil, burnt areas and secondary land cover for tracks with bare land cover)	11

Training synthetic spectral unmixing models requires training data covering all potential mixtures of endmember classes. We implemented the approach outlined in Cooper et al., 2020 and Okujeni et al., 2021 to create a synthetic training dataset from the above described pure endmembers that can be used as input for model training. A total of 15 training datasets were produced by creating five distinct synthetically mixed training datasets for each of the three target classes - tree cover, bare ground and shrubs/grassland. Each dataset contained 1000 synthetic mixtures at random mixing ratios (e.g., 80% tree cover, 20% bare ground), which represent the weighted averages of pure spectral signatures. We employed a maximum mixing complexity of three classes, with 20% of mixtures being one-class mixtures, 50% being two-class and 30% being three-class mixtures. These mixtures were generated by combining the spectral-temporal metrics (see 3.1) with cover proportions ranging from 0 to 1. This approach ensured that the regression model could accurately predict cover proportions across the entire spectrum present in our study system. Class likelihoods were determined by the proportional share of class entries in the library. Finally, the synthetic mixture was calculated as a linear combination of the selected spectral-temporal metrics, weighted by the assigned mixing proportions. The generation of synthetic training data was conducted using the FORCE synthmix module (Frantz, 2019).

These synthetical training datasets, along with their respective mixing ratios, were then used to train regression models predicting annual fractional cover of each land cover type (Okujeni et al., 2017; Okujeni et al., 2013). For each target class, five regression models were trained using resampled training data. This technique leads to five intermediate predictions per pixel and target class, which were averaged to obtain a final prediction. This method, known as ensemble approach, has been demonstrated to enhance prediction robustness (Okujeni et al., 2017). We used support vector regression (Smola and Schölkopf, 2004) and optimized model parameters via 10-fold cross-validation grid search. The ensemble of support vector regression models was then applied annually to all pixels, resulting in annual predictions of tree cover, bare ground, and shrubs/grassland cover fractions at disturbed sites over the years 1990 to 2021.

To validate our fractional cover maps, we compared them to visual estimates based on high-resolution aerial imagery. Additional information on the high-resolution imagery used in this study can be found in Table S1. We randomly selected 100 pixels, ensuring a minimum distance of 90 m between each to avoid selecting neighbouring pixels. Within each 30 m × 30 m pixel, we distributed 3 × 3 points evenly. These points were visually assigned to discrete labels of tree cover, bare ground, or shrubs/grassland. If a pixel represented a land cover class that couldn't be assigned (e.g., water), it was excluded, and a new one

was randomly chosen. Subsequently, we calculated sample proportions for each class to estimate the reference fractions. To evaluate the agreement between predicted and reference class fractions, we generated scatterplots and assessed the model fit with standardized major axis regression (SMA) and the coefficient of determination (R^2). We further validated our results based on the Mean Absolute Error (MAE) and the Relative Root Mean Squared Error (rRMSE), with the latter being normalized by the value range. Confidence intervals were obtained using bootstrapping with 1000 iterations. To quantify how uncertainties in tree cover estimates will percolate into estimates of recovery, we employed a Monte Carlo simulation to create 100 random draws of tree cover estimates from a normal distribution around the estimated value with the standard deviation corresponding to the MAE. The resulting draws provide insights into the range of possible outcomes under prediction uncertainty and the associated uncertainties in subsequent estimates (i.e., recovery intervals as described below).

3.3. Recovery analysis

3.3.1. Estimating post-disturbance recovery intervals

We used the annual tree cover fraction maps derived from spectral unmixing as described above to compute disturbance severity and analyse post-disturbance recovery. For doing so, we first randomly sampled 500,000 pixels for subsequent analysis to reduce the amount of and redundancy in data and speed up calculations. As we were primarily interested in regional estimates, this step does not lead to lower precision, because sampling uncertainty will be small given that the sample is still large (500,000 pixels times 32 years totalling to 16 million observations). Second, we used the year of disturbance (see chapter 2; Senf and Seidl, 2021) as a starting point of analyses. In many cases, however, the disturbance year did not correspond exactly to the year of minimum post-disturbance tree cover and thus with the start of the recovery signal (see Fig. 2). We thus identified the year of minimum tree cover within two years before and after the disturbance and used this year as starting point for all following analyses.

To analyse the potential impact of disturbance severity on recovery intervals, we calculated the relative difference between minimum post-disturbance tree cover and average tree cover over all the available years before disturbance, thus representing the percentual change in tree cover over the disturbance event (see Fig. 2). We used disturbance severity to subdivide disturbances into stand-replacing ($\geq$ 80% canopy loss) and non-stand-replacing disturbances (<80% canopy loss). Additionally, we conducted a comparative analysis between our tree cover-based severity measures and the widely used differenced Normalized Burn Ratio (dNBR) to test if both metrics capture the entire range of severity levels.

Before calculating recovery intervals, we smoothed out year-to-year variation in the tree cover estimates using generalized additive models with splines using 3 knots (see Fig. 2). This step was necessary as random year-to-year variation can lead to random observations crossing the recovery threshold even though average conditions do not indicate recovery. From the GAM-derived tree cover fractions, we calculated recovery intervals based on definitions given in Ingrisch and Bahn, 2018: absolute recovery and baseline-normalized recovery. The former sets a fixed threshold independent of pre-disturbance conditions, whereas the latter sets a pre-disturbance reference level ("baseline") as recovery threshold. For absolute recovery, we relied on the FAO definition of closed forests, which requires a minimum tree cover of 40% (FAO, 2012). For baseline-normalized recovery, we set the baseline as 80% of the average pre-disturbance tree cover, in accordance with most previous studies employing spectral indices (White et al., 2022). We then calculated the time required to reach this threshold after disturbance, following defined as recovery interval. The definition of baseline-normalized recovery is particularly useful when comparing different ecosystems and disturbance agents, as it measures the disturbance response relative to the pre-disturbed state (Ingrisch and Bahn, 2018), whereas the absolute recovery can be used to implement existing definitions (i.e. FAO forest definition in our case). We also calculated baseline-normalized recovery intervals for time series of NBR and NDVI to make our approach comparable to previous studies. Specifically, we used the 75th percentile of annual NBR and NDVI values (corresponding to summer conditions), applying 80% of the average pre-disturbance

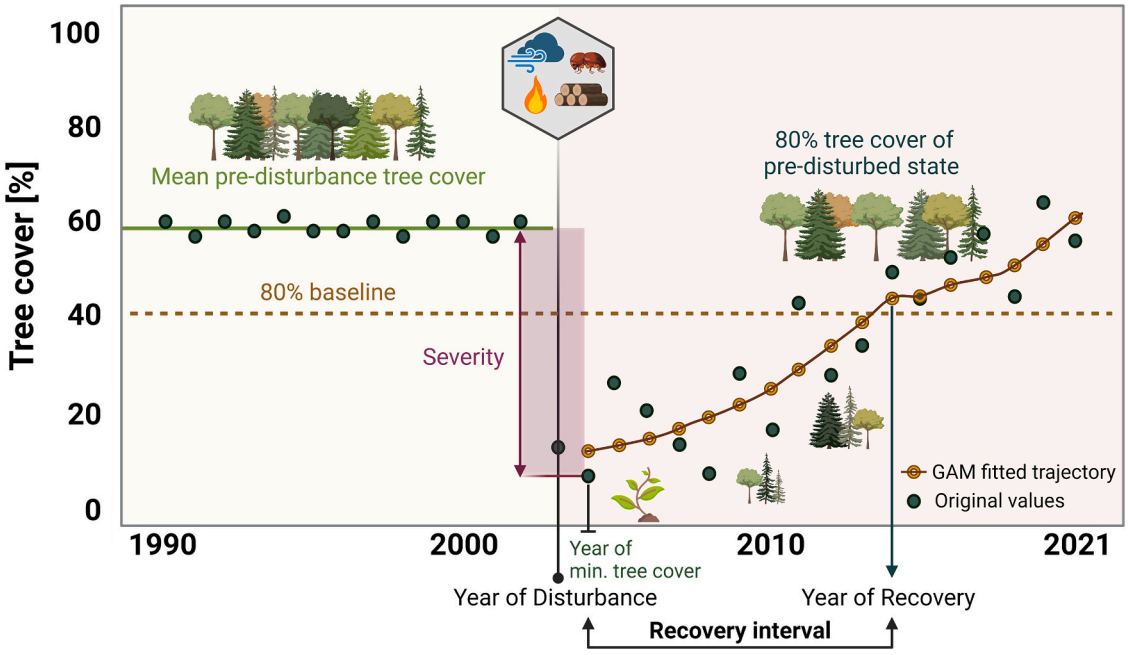

Fig. 2. Exemplary trajectory from real data showing the pre-disturbance tree cover (green solid line), the 80% baseline (brown dashed line), severity (purple) as well as the year of disturbance and the year of recovery. The time between the year of minimum tree cover within ±2 years before/after disturbance and the year of recovery is the recovery interval. Dark green dots after the disturbance represent the tree cover values from fractional cover maps, the yellow dots and the yellow line show the GAM-fitted trajectory, aiming for reducing inter-annual variations. Created with BioRender.com. (For interpretation of the references to colour in this figure legend, the reader is referred to the web version of this article.)

NBR and NDVI values as baseline for recovery (i.e. as suggested by White et al., 2018; White et al., 2017 and White et al., 2022). Calculating absolute recovery from the spectral indices was not possible, as there is no general spectral threshold indicating forest recovery. Finally, in addition to recovery intervals (i.e. the time from minimum tree cover to recovery), we also calculated the proportion of pixels recovered within 10, 20 and 30 years after disturbance.

3.3.2. Predicting long-term recovery success

The last objective of our study was to test whether we can predict long-term recovery success based on disturbance characteristics and post-disturbance bare ground fractions derived from spectral unmixing. We approached this objective by predicting the probability of recovery 10 years after disturbance using both relative and absolute recovery indicators. For prediction, we used logistic regression with the following predictors: pre-disturbance average tree cover, disturbance severity, and the fraction of bare ground three years after disturbance. Pre-disturbance tree cover is expected to represent the baseline ecological state of an ecosystem, impacting its ability to recover after disturbances with greater tree cover associated with greater capacity to recover due to seed availability and favourable microclimate conditions (Vandewiele et al., 2023; Zehetgruber et al., 2017). Disturbance severity is regarded as a key determinant of the magnitude of ecological disruption (Izquierdo et al., 2023) and is assumed to have strong implications for recovery trajectories because it determines the amount of live trees carried over into the post-disturbance state. The bare ground share shortly after the disturbance event may reflect soil degradation and vegetation loss of disturbed sites and thus the temporary disruption of forest structure. High levels of bare ground share may indicate a delayed or impeded recovery process, as vegetation regrowth is hindered by the absence of plant cover (Mantero et al., 2023).

The accuracy of the model was assessed using 5-fold cross validation and the optimal probability threshold for deriving a binary prediction from the continuous probability was optimized using the F1-score. We further explored potential interactions between the fractions of bare ground and pre-disturbance tree cover and bare ground and disturbance severity. We also tested the robustness of the model for predicting recovery success 15-, 20- and 30- years post disturbance and report the results in Fig. S7.

4. Results

4.1. Annual fraction mapping – accuracy and uncertainty

We observed high agreement between the fractional cover maps and the validation data, with R^2 values of 0.88 for tree cover, 0.93 for bare ground, and 0.74 for shrubs/grassland (Fig. 3). The mean absolute errors were 10.6% for tree cover, 4.2%for bare ground, and 14.8% for shrubs/grassland. The scatterplots demonstrated a strong linear relationship across all classes, with no signs of saturation at the extremes, but a tendency of underestimation of all fractional cover classes compared to visual interpretation.

The average pre-disturbance tree cover across all pixels was 67%, with 81% of the pixels having a tree cover between 40 and 100% and thus representing closed canopy conditions. Using average pre-disturbance tree cover and minimum post-disturbance tree cover, we estimated an average disturbance severity of 71% canopy loss during disturbance (see Fig. 4). Stand-replacing-disturbances (defined as severity >80% canopy loss) accounted for 49% of all disturbed pixels. For an exemplary map of pre- and post-disturbance tree cover, see Fig. S8. Comparing the severity measured through canopy loss with dNBR, a widely used measure of severity, we found a non-linear relationship between both metrics where dNBR consistently underestimates severity and has only very limited potential to capture low severity disturbances (see Fig. S9).

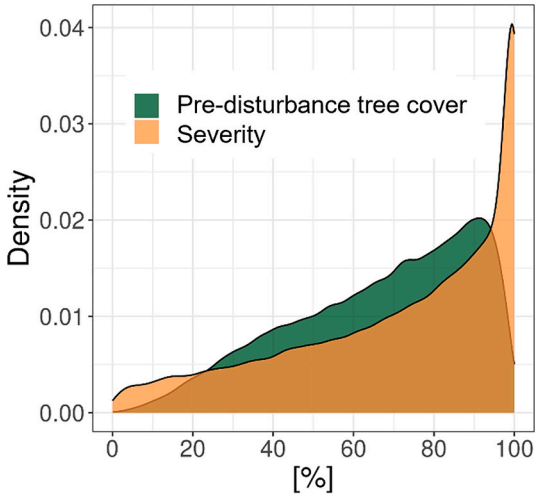

Fig. 4. Distribution of pre-disturbance tree cover and severity in the eastern Alps.

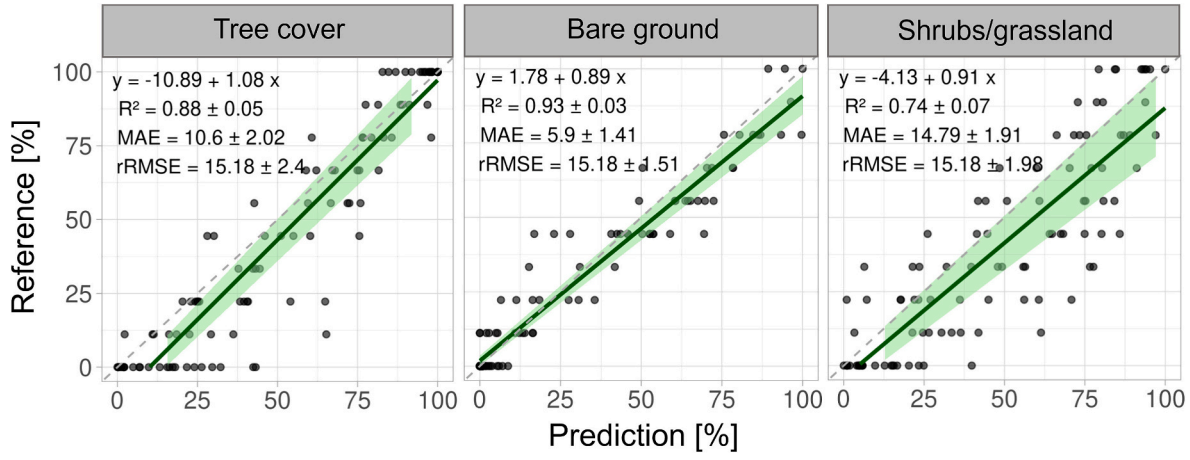

Fig. 3. Predicted versus observed fractions of tree cover, bare ground, and shrubs/grassland. The grey dashed lines show the 1:1 line, the green lines a linear regression fits. 95% confidence intervals were derived by bootstrapping. (For interpretation of the references to colour in this figure legend, the reader is referred to the web version of this article.)

4.2. Objective 1: post-disturbance recovery intervals

We quantified the recovery intervals for tree cover- and spectral-index based recovery indicators across our full study system and stratified by non-stand-replacing and stand-replacing disturbances (using the 80% severity threshold defined above). The distribution of recovery intervals was right-skewed for non-stand-replacing disturbances, but more normally distributed for stand-replacing disturbances. The mean post-disturbance recovery interval for tree cover-based absolute recovery was 5.5 ± 0.03 years (mean and standard error) for non-stand-replacing disturbances and 13.4 ± 0.16 years for stand replacing disturbances. For tree cover-based baseline-normalized recovery (i.e. reaching 80% of pre-disturbance tree cover), we found a mean recovery interval of 6.9 ± 0.04 years for non-stand-replacing disturbances and 10.2 ± 0.64 years for stand-replacing disturbances. The use of spectral index-based indicators, in turn, showed substantially faster recovery intervals. Baseline-normalized recovery in NBR displayed recovery intervals of 3.5 ± 0.01 years for non-stand-replacing disturbances and 7.3 ± 0.36 years for stand-replacing disturbances. NDVI-based recovery intervals were even shorter, averaging to 1.6 ± 0.006 years for non-stand-replacing disturbances and 5.9 ± 0.32 years for stand-replacing disturbances (see Fig. 6a). For uncertainty analyses using Monte Carlo simulations, please see Fig. S10.

Over the full observation period of 32 years, almost all disturbances (97%) recovered according to the tree cover-based absolute recovery definition, compared to 95% for tree cover-based baseline-normalized recovery definition (Fig. 5b). By reducing the observation period to 20 years post-disturbance, approximately 95% of forests showed recovery using the absolute recovery definition, while about 93% did so for the baseline-normalized definition. In contrast, only 71% and 60% of all disturbed pixels recovered within a decade for absolute and baseline-normalized recovery, respectively. Comparing those results to spectral index-based indicators, we found recovery success for 100% of all disturbances over our 32-year observation period, as well as within the 20-year time window for both NBR and NDVI-based recovery. Focusing on recovery 10 years post-disturbance, 83% recovered for the NBR-based recovery indicator while 93% of forests exhibited recovery for the NDVI-based definition (see Fig. 5b). Recovery based on spectral indices was thus far more rapid than recovery measured in terms of canopy cover.

In Fig. 6, we illustrate the derivation of recovery intervals from fractional cover maps using the example of a storm (2008) in Črnivec, SIovenia. The storm event in Črnivec resulted in a very high severity (mean of 91% canopy loss). We estimated a mean recovery interval of 5.6 years for absolute recovery and 8.8 years for baseline-normalized recovery. Areas with high pre-disturbed tree cover showed rapid recovery, resulting in an 82% recovery success within the observation period (2008–2021) for absolute recovery. For baseline-normalized recovery, however, we estimate that only 26% of all pixels recovered until 2021 and thus within 13 years post-disturbance.

4.3. Objective 2: predicting long-term recovery success

Using pre-disturbance tree cover, disturbance severity and post-disturbance bare ground fractions as predictors allowed us to predict the probability of recovery ten years post disturbance. For absolute recovery, the overall model accuracy was 83%, with an error of commission of 22%, an error of omission of 5%, and an F1 score of 0.79. Baseline-normalized recovery was predicted with similar overall accuracy of 76%, an error of commission of 7%, an error of omission at 17%, and an F1 score of 0.67. Predictions of recovery success over longer time periods (20 and 30 years) had similar accuracies (see Fig. S7), thus

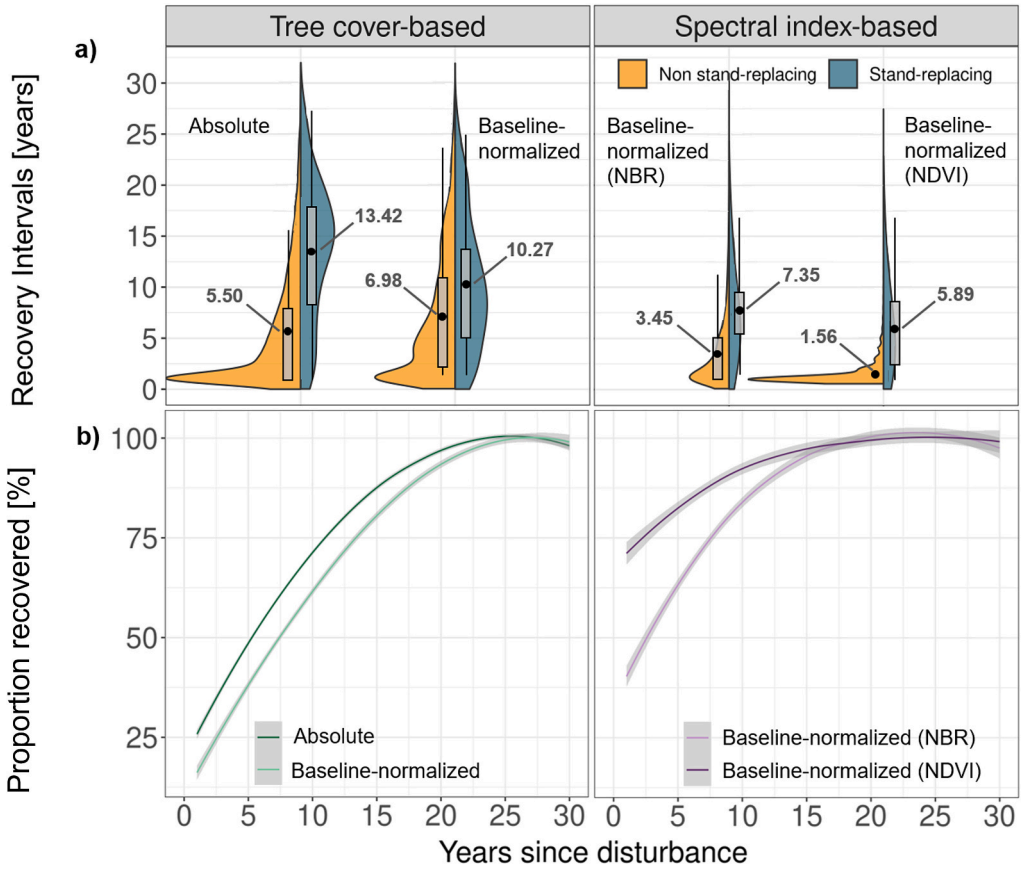

Fig. 5. Recovery intervals stratified by disturbance type (a) and percentage of recovered disturbances (b) for different indicators of recovered disturbances. Please note, that subplot a) and b) are independent plots, thus not sharing a common x-axis.

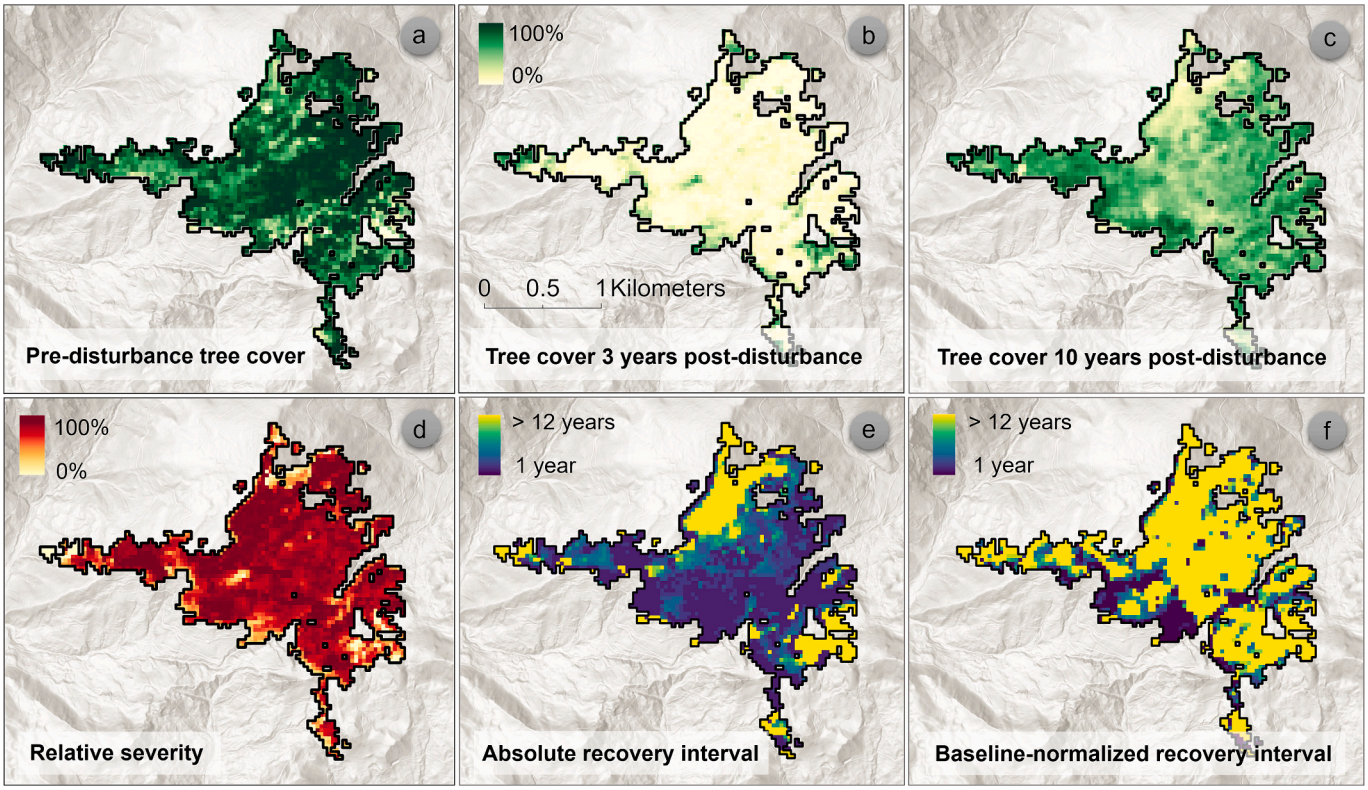

Fig. 6. Example for recovery from a storm event in Črnivec, SIovenia, occurring in the year 2008. The first row displays the development of tree cover from pre-disturbance (a) to immediately post-disturbance (b), and finally to 10 years post-disturbance state (c). The second row shows the severity (d), along with maps of the two recovery definitions: absolute recovery (i.e. reaching >40% tree cover; e) and baseline-normalized recovery (i.e. reaching >80% pre-disturbance tree cover; f). The area shown here refers to location (b) in Fig. 1.

representing stable recovery estimates over time. The observed and predicted recovery success (Fig. 7) showed a similar spatial pattern, where lower pre-disturbance tree cover value, high disturbance severity and a high bare ground share led to reduced recovery probabilities. We thus provide evidence that recovery success can be predicted successfully from the patterns emerging in the first three years after disturbance.

Investigating the effects of each predictor as well as their interactions, we found a higher probability of recovery for the absolute recovery indicator in areas with high pre-disturbance tree cover and low bare ground shares, while baseline-normalized recovery was more likely in areas with a lower pre-disturbance cover (Fig. 8). We observed a similar relationship between relative severity and bare ground share three years post-disturbance: The probability of successful recovery increased as the bare ground share and relative severity decreased, which was consistent for both recovery indicators. With high shares of bare ground three years post-disturbance, the probability of recovery is severely reduced across all levels of pre-disturbance cover and disturbance severity.

5. Discussion

We here present a new approach for determining post-disturbance forest recovery intervals and predicting long-term recovery success based on ecologically informed disturbance and recovery characteristics. We found strong differences in recovery between recovery definitions (i.e. absolute or baseline-normalized) and between stand-replacing and non-stand-replacing disturbances. Absolute recovery definitions use a fixed tree cover threshold that has to be reached after disturbance, such as 40% as defined for close-canopy forests by the FAO (FAO, 2012). While using a fixed threshold has advantages (e.g. comparable across regions), recovery intervals can be substantially influenced by pre-disturbance tree cover: In systems characterized by dense forests, for instance, a fixed threshold can be reached very quickly post-disturbance, or low disturbance severities might not even push tree cover below the predefined threshold at all. However, in a system characterized by open forests, commonly occurring in high elevation forests or drier regions of the world (Stritih et al., 2023), a fixed threshold might never be met. Baseline-normalized recovery, in contrast, is more adaptive to variable pre-disturbance tree covers and disturbance severities, as it directly considers pre-disturbance tree cover in its definition. While non-stand-replacing disturbances still lead to shorter recovery intervals, the proportional nature of this indicator causes a smaller difference between the two disturbance types compared to absolute recovery. The different underlying mechanisms of these recovery indicators are also reflected in the consistently higher proportion of recovered pixels for absolute recovery compared to baseline-normalized recovery, which corresponds with findings by Bartels et al. (2016). The differences between recovery definitions shown here highlight the need for carefully choosing and explicitly defining recovery in remote sensing studies. Our results further highlight that disturbance characteristics themselves impact recovery estimates, and reporting recovery estimates without a quantification of disturbance severity might be misleading.

We found high variability in spectral recovery intervals estimated from NDVI and NBR, with variability likely linked to the spectral index, disturbance characteristics and also the heterogeneity of the study system. Our findings indicate that spectral index-based recovery metrics, if used as surrogate for canopy cover, estimated considerably lower recovery intervals than our tree cover-based indicators for both stand-replacing and non-stand-replacing disturbances. Comparing our results to existing studies, Pickell et al., 2016 found a mean spectral recovery length of 5.6 years for NBR and 2.7 years for NDVI in North American boreal forests, which is similar to the recovery intervals we found for NBR (4.9 years) and NDVI (3.3 years) for our system. Focusing on fire-

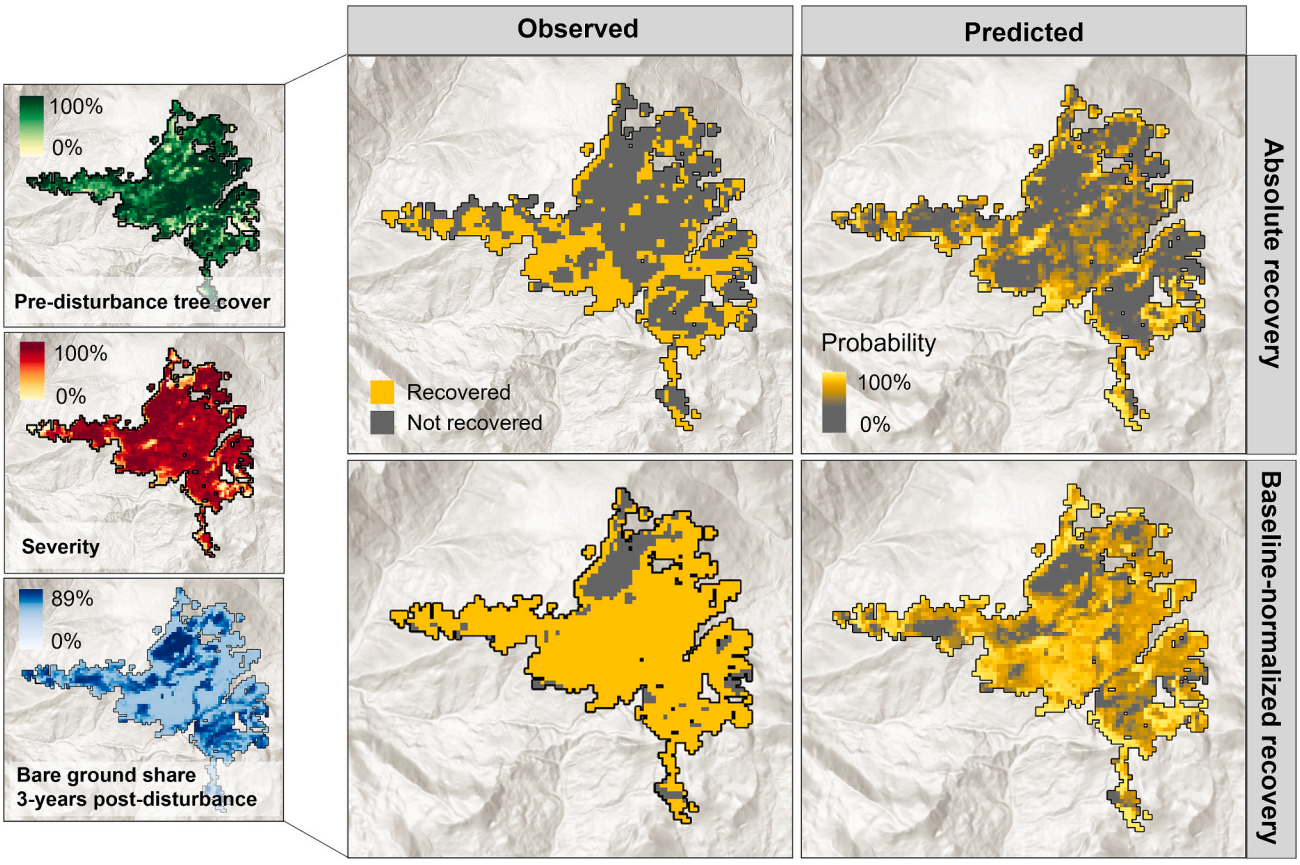

Fig. 7. Mapped predictors (see also Fig. 5) used as input for the logistic regression model, which are translated into probabilities of recovery success (right). The column in the middle shows observed recovery success derived from the fractional cover maps.

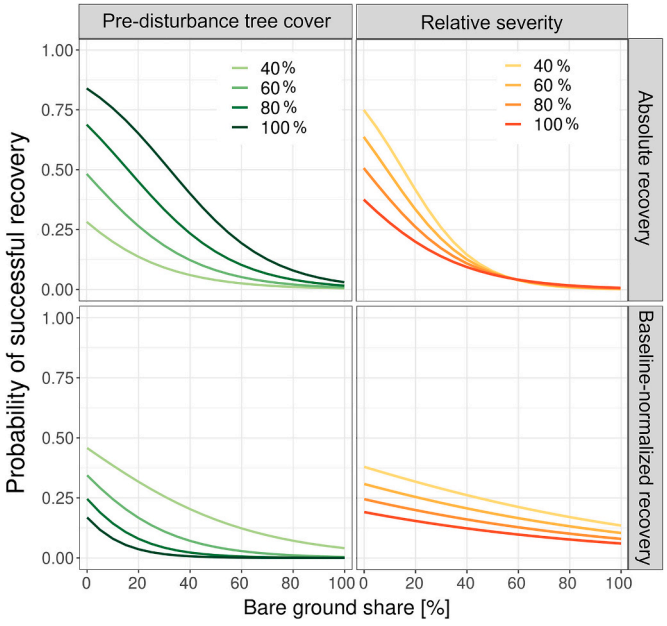

Fig. 8. Effects of pre-disturbance tree cover, relative severity and bare ground share three years post-disturbance on the probability of absolute and baseline-normalized recovery 10 years post-disturbance (for other time frames see Figs. S7 and S12).

prone forests in Australia, Hislop et al., 2018 observed comparatively longer recovery intervals, specifically eight years for NBR and five years for NDVI. Examining Canada's forested ecosystems, particularly impacted by wildfires and harvest, White et al., 2022 reported recovery intervals for baseline-normalized NBR ranging from 6.1 years (harvest) to 10.6 years (fires). This is substantially longer than in our study, but disturbances in this particular study were also larger than average disturbance patches in Europe, which may slow recovery due to limited seed supply (Hansen et al., 2018). In a different context (coppice forests), Chirici et al., 2020 found no substantial differences between NDVI and NBR recovery. In our study system, characterized by a combination of natural and human disturbances and more complex spectral signals due to the small-scale nature and patchiness of disturbances (Maroschek et al., 2023), NDVI led to consistently shorter recovery intervals compared to NBR, aligning with the conclusion of Hislop et al., 2018 and Pickell et al., 2016. The substantially shorter recovery intervals observed for spectral-index based metrics compared to tree cover-based metrics may be attributed to the underestimation of disturbance severity with dNBR compared to canopy cover (Fig. S9), which is likely related to residual trees on non-stand-replacing disturbances that lead to higher post-disturbance vegetation index values compared to post-disturbance canopy cover estimates. Finally, a common drawback of using a spectral-index-based approach is the lack of specific details about which land cover class drives the increase in the spectral index. Not only tree regrowth, but also the presence of other vegetation (grasses and shrubs) can quickly increase photosynthetic activity on disturbed sites (Buma, 2012), without leading to forest recovery in the sense of reaching a pre-disturbance tree cover state. Spectral indices should thus only be seen as proxies for physical and functional recovery (Helfenstein et al., 2022), but not taken as proxy of post-disturbance canopy recovery.

Our newly developed recovery indicators, based on clearly defined ecological units (percent tree cover, percent recovery to pre-disturbance tree cover), overcomes difficulties in interpretability of spectral recovery indicators and likely result in more realistic estimates of post-

disturbance canopy recovery. While our study focuses on one structural dimension of recovery (i.e. canopy cover), it is important to recognize that other dimensions, such as tree height or species composition, have not been incorporated into our analysis. We assume longer recovery times when additional dimensions are considered, which is supported by a study from Stritih et al., 2023, showing that tree cover recovered faster than tree height in mountain forests. Incorporating multiple dimensions of recovery into our analysis could offer a more comprehensive perspective on forest recovery. For example, variation in tree height can be used as an indicator of forest developmental stage, while, changes in species composition can provide insights into shifts in ecological communities and habitat suitability over time, offering a nuanced understanding of ecosystem services and dynamics (Stritih et al., 2021a). Nevertheless, while recognizing the potential benefits of integrating multiple dimensions recovery assessments, they are also associated with practical challenges. One significant obstacle is the lack of time series from LiDAR data, which would allow for assessing detailed information on forest structure, as well as a lack of temporal information on tree species (Blickensdörfer et al., 2024).

Our spectral unmixing approach allowed us to investigate how post-disturbance land cover and disturbance characteristics influence forest recovery. For post-disturbance land cover, we found a negative relationship between an increasing bare ground share shortly after disturbance and a decreasing probability of successful recovery. Ecologically, this might be attributed to several factors: A high bare ground share indicates a complete loss of vegetation, including early and advanced regeneration, often caused by mechanized salvage logging operations. This loss of vegetation potentially leads to reduced seed availability from remaining trees and soil seed banks. The latter is especially noticeable after wildfires and salvage logging (Brown and Johnstone, 2012; Leverkus and Castro, 2017). Dispersal of seeds from nearby areas and refilling of the soil seed bank takes a significant amount of time (Bowd et al., 2019; Ibáñez et al., 2019), which in turn leads to delayed recovery. An increased bare ground share can also induce changes in the microclimate, as the buffering effect provided by vegetation is lost (Bugalho et al., 2011; Vandewiele et al., 2023). More extreme temperature fluctuations and lower soil moisture create suboptimal conditions for seed germination and establishment (Vieira and Scariot, 2006). Finally, soil compaction and erosion have a negative impact on tree establishment and growth (Marchi et al., 2016; Meyer et al., 2014). Compacted soil restricts root development, hindering a trees' ability to anchor itself and access nutrients and water. Erosion exacerbates this challenge by removing the top layer of the soil, which is rich in organic matter and essential nutrients necessary for supporting the regrowth of trees (Quinton et al., 2010). Post-disturbance bare ground fractions can thus be identified as an important early predictor of long-term recovery success.

Considering disturbance characteristics, pixels with a higher pre-disturbance tree cover are more likely to reach absolute recovery thresholds, but less likely to recover under a baseline-normalized recovery definition. This discrepancy between recovery definitions arises because absolute recovery ignores the pre-disturbance characteristics of forests, whereas baseline-normalized recovery takes them into account. In the case of absolute recovery, the requirement to reach the 40% tree cover threshold implies that higher pre-disturbance tree cover acts as a facilitator for recovery success. For baseline-normalized recovery, a lower pre-disturbance tree cover might indicate increased light availability, promoting the growth of understory vegetation and facilitating advanced regeneration (Stiers et al., 2019). Lower competition for resources in open forests enhances effective seed dispersal and allows for faster growth rates and easier establishment of pioneer species, which might support a quicker recovery process (Damptey et al., 2023). The consistent trend of lower recovery probability with higher disturbance severity can be explained by the simple fact that with lower disturbance severities, there are more residual trees and the site will thus meet recovery thresholds more quickly (Stuart-Haëntjens et al., 2015).

The results of our study suggest that the efficient monitoring of forest recovery can be achieved by assessing pre- and early post-disturbance characteristics, reducing the need for long-term time series to estimate recovery. This is important because it allows managers to counteract potentially undesirable trajectories (e.g., by tree planting) before they unfold, without having to first wait for the undesired outcome to materialize. Our novel approach thus goes beyond past remote sensing-based studies on forest recovery, which required long time series to track recovery trajectories over extended periods post-disturbance (ten or more years; Chirici et al., 2020; Senf and Seidl, 2022; Smith-Tripp et al., 2024; White et al., 2022; White et al., 2018). Our findings show that early post-disturbance indicators already provide crucial insights into long-term recovery of the forest canopy. The capability of our approach to promptly monitor forest recovery based on disturbance characteristics and early post-disturbance indicators substantially improves our capacity to support management decisions with remote sensing. With access to up-to-date information on recovery shortly after disturbance, forest managers can quickly react, e.g. through the identification of areas that require intervention, allowing for targeted reafforestation efforts to promote recovery in areas that show signs of delayed or compromised recovery. Nonetheless, it's important to acknowledge that in this study, we examined canopy recovery, which is only one dimension of forest recovery (see discussion above). In contrast to many studies that focus on small study sites or specific disturbance agents such as fire (e.g. Bousquet et al., 2022, Pérez-Cabello et al., 2021, Pfoch et al., 2023; Smith-Tripp et al., 2024 or Viana-Soto et al., 2022), and studies investigating particular management scenarios, like productive forests in Finland (White et al., 2018), we here analyse recovery across a large and complex area with diverse disturbance agents and management strategies. Our results are thus likely transferable also to other regions. Monitoring recovery over time also allows for the identification of early warning indicators (Seidl and Turner, 2022), potentially signaling eroding resilience in forests frequently affected by forest disturbances (Reyer et al., 2015).

6. Conclusion

We here present a new approach for estimating post-disturbance forest recovery intervals and predicting long-term recovery success from remote sensing data. Based on our findings, we arrive at four conclusions: (1) Traditional spectral index-based recovery indicators - if taken as proxies for tree cover - substantially underestimated recovery intervals compared to tree cover-based indicators derived from spectral unmixing. (2) Disturbance severity has a major influence on post-disturbance recovery; recovery studies thus should consider disturbance characteristics explicitly. (3) The majority of forests in the Alps recover their tree cover within three decades post disturbances. (4) Pre- and early post-disturbance characteristics can predict long-term (ten-year) recovery success, suggesting that recovery trajectories can be gleaned from the short window of post-disturbance forest reorganization. Our study emphasizes the effectiveness of remote sensing for assessing forest recovery, yet it also highlights that recovery indicators need to be ecologically informed and well defined in order to be applicable and comparable across studies. Our newly developed approach predicting long-term recovery success based on pre- and early post-disturbance characteristics further facilitates the monitoring of post-disturbance recovery as an important component of forest resilience, which is direly needed in a rapidly changing world.

Author contributions

Conceptualization: LM and CS; Investigation: LM, AVS, AS, CS; Formal analysis: LM; Methodology: LM, AVS, AS, RS, CS; Writing - original draft: LM; Writing - review & editing: AVS, AS, RS, CS (editing).

Declaration of competing interest

The authors declare no competing interests.

Data availability

Data will be made publicly available after publication. The disturbance maps used are openly available and can be downloaded here: https://zenodo.org/records/7080016.

Acknowledgements

LM and CS acknowledge funding from the Fachagentur Nachwachsende Rohstoffe e.V. (FNR) through the ERA-Net cofound action ForestValue (project FORECO, projectnr. 2221NR088X). AVS acknowledges funding from the European Union's Horizon Europe Research and Innovation Programme as well as from the United Kingdom Research and Innovation Council (project ForestPath, projectnr. 101056755). RS acknowledges support from the European Research Council (ERC) under the European Union's Horizon 2020 research and innovation programme (grant agreement no. 101001905, FORWARD). We thank Katja Kowalski and Akpona Okujeni for sharing their valuable experience with synthetic spectral unmixing. Open access funding enabled and organized by Project DEAL.

Appendix A. Supplementary data

Supplementary data to this article can be found online at https://doi.org/10.1016/j.rse.2024.114194.

References

Alfaro-Sánchez, R., Camarero, J.J., López-Serrano, F.R., Sánchez-Salguero, R., Moya, D., Heras, J.D.L., 2015. Positive coupling between growth and reproduction in young post-fire Aleppo pines depends on climate and site conditions. Int. J. Wildland Fire 24, 507–517.

Bartels, S.F., Chen, H.Y.H., Wulder, M.A., White, J.C., 2016. Trends in post-disturbance recovery rates of Canada's forests following wildfire and harvest. For. Ecol. Manag. 361, 194–207.

Bebi, P., Seidl, R., Motta, R., Fuhr, M., Firm, D., Krumm, F., Conedera, M., Ginzler, C., Wohlgemuth, T., Kulakowski, D., 2017. Changes of forest cover and disturbance regimes in the mountain forests of the Alps. For. Ecol. Manag. 388, 43–56.

Beloiu, M., Stahlmann, R., Beierkuhnlein, C., 2022. Drought impacts in forest canopy and deciduous tree saplings in central European forests. For. Ecol. Manag. 509, 120075.

Blickensdörfer, L., Oehmichen, K., Pflugmacher, D., Kleinschmit, B., Hostert, P., 2024. National tree species mapping using Sentinel-1/2 time series and German national forest inventory data. Remote Sens. Environ. 304, 114069.

Bohn, U., Gollub, G., Hettwer, C., Weber, H., Neuhäuslová, Z., Raus, T., Schlüter, H., 2000. Karte der natürlichen Vegetation Europas / Map of the Natural Vegetation of Europe - Maßstab / Scale 1:2,500,000.

Bousquet, E., Mialon, A., Rodriguez-Fernandez, N., Mermoz, S., Kerr, Y., 2022. Monitoring post-fire recovery of various vegetation biomes using multi-wavelength satellite remote sensing. Biogeosciences 19, 3317–3336.

Bowd, E.J., Banks, S.C., Strong, C.L., Lindenmayer, D.B., 2019. Long-term impacts of wildfire and logging on forest soils. Nat. Geosci. 12, 113–118.

Brown, C.D., Johnstone, J.F., 2012. Once burned, twice shy: repeat fires reduce seed availability and alter substrate constraints on *Picea mariana* regeneration. For. Ecol. Manag. 266, 34–41.

Bugalho, M.N., Lecomte, X., Gonçalves, M., Caldeira, M.C., Branco, M., 2011. Establishing grazing and grazing-excluded patches increases plant and invertebrate diversity in a Mediterranean oak woodland. For. Ecol. Manag. 261, 2133–2139.

Buma, B., 2012. Evaluating the utility and seasonality of NDVI values for assessing post-disturbance recovery in a subalpine forest. Environ. Monit. Assess. 184, 3849–3860.

Buschmann, C., Nagel, E., 1993. In vivo spectroscopy and internal optics of leaves as basis for remote sensing of vegetation. Int. J. Remote Sens. 14 (1993), 711–722.

Cerioni, M., Brabec, M., Bače, R., Bäders, E., Bončina, A., Brůna, J., Chećko, E., Cordonnier, T., de Koning, J.H.C., Diaci, J., Dobrowolska, D., Dountchev, A., Engelhart, J., Fidej, G., Fuhr, M., Garbarino, M., Jansons, Ā., Keren, S., Kitenberga, M., Klopčič, M., Konôpka, B., Kopecký, M., Köster, K., Kucbel, S., Lacombe, E., Laurent, L., Leyman, A., Lingua, E., Macek, M., Maciejewski, Z., Malandra, F., Marzano, R., Metslaid, M., Morresi, D., Panayotov, M., Pawlak, B., Pittner, J., Šebeň, V., Socha, J., Svoboda, M., Szwagrzyk, J., Tsvetanov, N., Urbinati, C., Vallet, P., Van de Kerckhove, P., Vandekerkhove, K., Vencurik, J., Vitali, A., Vodde, F., Wild, J., Nagel, T.A., 2024. Recovery and resilience of European temperate forests after large and severe disturbances. Glob. Chang. Biol. 30, e17159.

Chirici, G., Giannetti, F., Mazza, E., Francini, S., Travaglini, D., Pegna, R., White, J.C., 2020. Monitoring clearcutting and subsequent rapid recovery in Mediterranean coppice forests with Landsat time series. Ann. For. Sci. 77, 40.

Cooper, S., Okujeni, A., Jänicke, C., Clark, M., van der Linden, S., Hostert, P., 2020. Disentangling fractional vegetation cover: regression-based unmixing of simulated spaceborne imaging spectroscopy data. Remote Sens. Environ. 246, 111856.

Damptey, F.G., Adofo, E., Duah-Gyamfi, A., Adusu, D., Opuni-Frimpong, E., 2023. Logging effects on seedling regeneration and diversity in a tropical moist semi-deciduous forest in Ghana. Geol. Ecol. Landsc. 7, 269–280.

d'Andrimont, R., Yordanov, M., Martinez-Sanchez, L., Eiselt, B., Palmieri, A., Dominici, P., Gallego, J., Reuter, H.I., Joebges, C., Lemoine, G., van der Velde, M., 2020. Harmonised LUCAS in-situ land cover and use database for field surveys from 2006 to 2018 in the European Union. Sci. Data 7, 352.

FAO, 2012. Forest Resources Assessment Working Paper 180 – Terms and Definitions.

Frantz, D., 2019. FORCE—Landsat + Sentinel-2 analysis ready data and beyond. Remote Sens. 11.

Frantz, D., Röder, A., Stellmes, M., Hill, J., 2016. An operational radiometric Landsat preprocessing framework for large-area time series applications. IEEE Trans. Geosci. Remote Sens. 54, 3928–3943.

Frantz, D., Haß, E., Uhl, A., Stoffels, J., Hill, J., 2018. Improvement of the Fmask algorithm for Sentinel-2 images: separating clouds from bright surfaces based on parallax effects. Remote Sens. Environ. 215.

Frazier, R.J., Coops, N.C., Wulder, M.A., Hermosilla, T., White, J.C., 2018. Analyzing spatial and temporal variability in short-term rates of post-fire vegetation return from Landsat time series. Remote Sens. Environ. 205, 32–45.

Frei, C., Schär, C., 1998. A precipitation climatology of the Alps from high-resolution rain-gauge observations. Int. J. Climatol. 18, 873–900.

Frolking, S., Palace, M.W., Clark, D.B., Chambers, J.Q., Shugart, H.H., Hurtt, G.C., 2009. Forest disturbance and recovery: a general review in the context of spaceborne remote sensing of impacts on aboveground biomass and canopy structure. J. Geophys. Res. Biogeosci. 114.

Gao, B.-C., 1996. NDWI—a normalized difference water index for remote sensing of vegetation liquid water from space. Remote Sens. Environ. 58, 257–266.

García, M.L., Caselles, V., 1991. Mapping burns and natural reforestation using thematic mapper data. Geocarto Int. 6, 31–37.

Gitas, I., Mitri, G., Veraverbeke, S., Polychronaki, A., 2012. Advances in Remote Sensing of Post-Fire Vegetation Recovery Monitoring - A Review.

Grantham, H.S., Duncan, A., Evans, T.D., Jones, K.R., Beyer, H.L., Schuster, R., Walston, J., Ray, J.C., Robinson, J.G., Callow, M., Clements, T., Costa, H.M., DeGemmis, A., Elsen, P.R., Ervin, J., Franco, P., Goldman, E., Goetz, S., Hansen, A., Hofsvang, E., Jantz, P., Jupiter, S., Kang, A., Langhammer, P., Laurance, W.F., Lieberman, S., Linkie, M., Malhi, Y., Maxwell, S., Mendez, M., Mittermeier, R., Murray, N.J., Possingham, H., Radachowsky, J., Saatchi, S., Samper, C., Silverman, J., Shapiro, A., Strassburg, B., Stevens, T., Stokes, E., Taylor, R., Tear, T., Tizard, R., Venter, O., Visconti, P., Wang, S., Watson, J.E.M., 2020. Anthropogenic modification of forests means only 40% of remaining forests have high ecosystem integrity. Nat. Commun. 11, 5978.

Haberl, H., Wiedenhofer, D., Schug, F., Frantz, D., Virág, D., Plutzar, C., Gruhler, K., Lederer, J., Schiller, G., Fishman, T., Lanau, M., Gattringer, A., Kemper, T., Liu, G., Tanikawa, H., van der Linden, S., Hostert, P., 2021. High-resolution maps of material stocks in buildings and infrastructures in Austria and Germany. Environ. Sci. Technol. 55, 3368–3379.

Hansen, W.D., Braziunas, K.H., Rammer, W., Seidl, R., Turner, M.G., 2018. It takes a few to tango: changing climate and fire regimes can cause regeneration failure of two subalpine conifers. Ecology 99, 966–977.

Helfenstein, I., Schneider, F.D., Schaepman, M., Morsdorf, F., 2022. Assessing biodiversity from space: impact of spatial and spectral resolution on trait-based functional diversity. Remote Sens. Environ. 275, 113024.

Hérault, B., Piponiot, C., 2018. Key drivers of ecosystem recovery after disturbance in a neotropical forest. For. Ecosyst. 5, 2.

Hermosilla, T., Wulder, M.A., White, J.C., Coops, N.C., 2019. Prevalence of multiple forest disturbances and impact on vegetation regrowth from interannual Landsat time series (1985–2015). Remote Sens. Environ. 233.

Hislop, S., Jones, S., Soto-Berelov, M., Skidmore, A., Haywood, A., Nguyen, T.H., 2018. Using Landsat spectral indices in time-series to assess wildfire disturbance and recovery. Remote 10, 460.

Huete, A.R., 1988. A soil-adjusted vegetation index (SAVI). Remote Sens. Environ. 25, 295–309.

Ibáñez, I., Acharya, K., Juno, E., Karounos, C., Lee, B.R., McCollum, C., Schaffer-Morrison, S., Tourville, J., 2019. Forest resilience under global environmental change: do we have the information we need? A systematic review. PLoS One 14, e0222207.

Ingrisch, J., Bahn, M., 2018. Towards a comparable quantification of resilience. Trends Ecol. Evol. 33, 251–259.

Izquierdo, L., Bengtsson, J., Clemmensen, K., Granath, G., Gundale, M., Ibáñez, T., Lindahl, B., Strengbom, J., Taylor, A., Viketoft, M., Wardle, D., Nilsson, M.-C., 2023. Fire severity as a key determinant of aboveground and belowground biological community recovery in managed even-aged boreal forests. Ecol. Evol. 13.

Jung, H., Senf, C., Beudert, B., Krueger, T., 2021. Bayesian hierarchical modeling of nitrate concentration in a forest stream affected by large-scale forest dieback. Water Resour. Res. 57 e2020WR027264.

Kleinman, J.S., Goode, J.D., Fries, A.C., Hart, J.L., 2019. Ecological consequences of compound disturbances in forest ecosystems: a systematic review. Ecosphere 10, e02962.

Kriegler, F.J., Malila, W.A., Nalepka, R.F., Richardson, W., 1969. Preprocessing Transformations and their Effects on Multispectral Recognition.

Leverkus, A.B., Castro, J., 2017. An ecosystem services approach to the ecological effects of salvage logging: valuation of seed dispersal. Ecol. Appl. 27, 1057–1063.
Liu, H.Q., Huete, A., 1995. A feedback based modification of the NDVI to minimize canopy background and atmospheric noise. IEEE Trans. Geosci. Remote Sens. 33, 457–465.
Liu, W., Guan, H., Hesp, P.A., Batelaan, O., 2023. Remote sensing delineation of wildfire spatial extents and post-fire recovery along a semi-arid climate gradient. Eco. Inform. 78, 102304.
Mantero, G., Morresi, D., Negri, S., Anselmetto, N., Lingua, E., Bonifacio, E., Garbarino, M., Marzano, R., 2023. Short-term drivers of post-fire forest regeneration in the Western Alps. Fire Ecol. 19, 23.
Marchi, E., Picchio, R., Mederski, P.S., Vusić, D., Perugini, M., Venanzi, R., 2016. Impact of silvicultural treatment and forest operation on soil and regeneration in Mediterranean Turkey oak (*Quercus cerris* L.) coppice with standards. Ecol. Eng. 95, 475–484.
Marcolin, E., Marzano, R., Vitali, A., Garbarino, M., Lingua, E., 2019. Post-fire management impact on natural forest regeneration through altered microsite conditions. Forests 10, 1014.
Maroschek, M., Seidl, R., Poschlod, B., Senf, C., 2023. Quantifying patch size distributions of forest disturbances in protected areas across the European Alps. J. Biogeogr. 51, 368–381.
McDowell, N.G., Allen, C.D., Anderson-Teixeira, K., Aukema, B.H., Bond-Lamberty, B., Chini, L., Clark, J.S., Dietze, M., Grossiord, C., Hanbury-Brown, A., Hurtt, G.C., Jackson, R.B., Johnson, D.J., Kueppers, L., Lichstein, J.W., Ogle, K., Poulter, B., Pugh, T.A.M., Seidl, R., Turner, M.G., Uriarte, M., Walker, A.P., Xu, C., 2020. Pervasive shifts in forest dynamics in a changing world. Science 368, eaaz9463.
Meyer, C., Lüscher, P., Schulin, R., 2014. Enhancing the regeneration of compacted forest soils by planting black alder in skid lane tracks. Eur. J. For. Res. 133, 453–465.
Nigrelli, G., Chiarle, M., 2023. 1991–2020 climate normal in the European Alps: focus on high-elevation environments. J. Mt. Sci. 20, 2149–2163.
Nikinmaa, L., Lindner, M., Cantarello, E., Jump, A.S., Seidl, R., Winkel, G., Muys, B., 2020. Reviewing the use of resilience concepts in forest sciences. Curr. For. Rep. 6, 61–80.
Okujeni, A., van der Linden, S., Tits, L., Somers, B., Hostert, P., 2013. Support vector regression and synthetically mixed training data for quantifying urban land cover. Remote Sens. Environ. 137, 184–197.
Okujeni, A., Linden, S.V.D., Suess, S., Hostert, P., 2017. Ensemble learning from synthetically mixed training data for quantifying urban land cover with support vector regression. IEEE J. Sel. Top. Appl. Earth Obs. Remote Sens. 10, 1640–1650.
Okujeni, A., Canters, F., Cooper, S.D., Degerickx, J., Heiden, U., Hostert, P., Priem, F., Roberts, D.A., Somers, B., van der Linden, S., 2018. Generalizing machine learning regression models using multi-site spectral libraries for mapping vegetation-impervious-soil fractions across multiple cities. Remote Sens. Environ. 216, 482–496.
Okujeni, A., Jänicke, C., Cooper, S., Frantz, D., Hostert, P., Clark, M., Segl, K., van der Linden, S., 2021. Multi-season unmixing of vegetation class fractions across diverse Californian ecoregions using simulated spaceborne imaging spectroscopy data. Remote Sens. Environ. 264, 112558.
Pecher, C., Tasser, E., Tappeiner, U., 2011. Definition of the potential treeline in the European Alps and its benefit for sustainability monitoring. Ecol. Indic. 11, 438–447.
Pérez-Cabello, F., Montorio, R., Alves, D.B., 2021. Remote sensing techniques to assess post-fire vegetation recovery. Curr. Opin. Environ. Sci. Health 21, 100251.
Pfoch, K.A., Pflugmacher, D., Okujeni, A., Hostert, P., 2023. Mapping forest fire severity using bi-temporal unmixing of Sentinel-2 data - towards a quantitative understanding of fire impacts. Sci. Remote Sens. 8, 100097.
Pickell, P.D., Hermosilla, T., Frazier, R.J., Coops, N.C., Wulder, M.A., 2016. Forest recovery trends derived from Landsat time series for North American boreal forests. Int. J. Remote Sens. 37, 138–149.
Quinton, J., Govers, G., Oost, K.V., Bardgett, R.D., 2010. The impact of agricultural soil erosion on biogeochemical cycling. Nat 3, 311–314.
Reyer, C.P.O., Brouwers, N., Rammig, A., Brook, B.W., Epila, J., Grant, R.F., Holmgren, M., Langerwisch, F., Leuzinger, S., Lucht, W., Medlyn, B., Pfeifer, M., Steinkamp, J., Vanderwel, M.C., Verbeeck, H., Villela, D.M., 2015. Forest resilience and tipping points at different spatio-temporal scales: approaches and challenges. J. Ecol. 103, 5–15.
Riggs, G.A., Hall, D.K., Salomonson, V.V., 1994. A snow index for the Landsat thematic mapper and moderate resolution imaging spectroradiometer. In: Proceedings of IGARSS '94–1994 IEEE International Geoscience and Remote Sensing Symposium, 1944, pp. 1942–1944.
Roy, D.P., Kovalskyy, V., Zhang, H.K., Vermote, E.F., Yan, L., Kumar, S.S., Egorov, A., 2016. Characterization of Landsat-7 to Landsat-8 reflective wavelength and normalized difference vegetation index continuity. Remote Sens. Environ. 185, 57–70.
Rüetschi, M., Weber, D., Koch, T.L., Waser, L.T., Small, D., Ginzler, C., 2021. Countrywide mapping of shrub forest using multi-sensor data and bias correction techniques. Int. J. Appl. Earth Obs. Geoinf. 105, 102613.
Rufin, P., Frantz, D., Yan, L., Hostert, P., 2021. Operational coregistration of the sentinel-2A/B image archive using multitemporal Landsat spectral averages. IEEE Geosci. Remote Sens. Lett. 18, 712–716.
Scheffer, M., Carpenter, S.R., Dakos, V., Nes, E.H.V., 2015. Generic indicators of ecological resilience: inferring the chance of a critical transition. Annu. Rev. Ecol. Evol. Syst. 46, 145–167.
Schug, F., Frantz, D., Okujeni, A., van der Linden, S., Hostert, P., 2020. Mapping urban-rural gradients of settlements and vegetation at national scale using Sentinel-2 spectral-temporal metrics and regression-based unmixing with synthetic training data. Remote Sens. Environ. 246.
Sebald, J., Senf, C., Heiser, M., Scheidl, C., Pflugmacher, D., Seidl, R., 2019. The effects of forest cover and disturbance on torrential hazards: large-scale evidence from the Eastern Alps. Environ. Res. Lett. 14, 114032.
Sebald, J., Senf, C., Seidl, R., 2021. Human or natural? Landscape context improves the attribution of forest disturbances mapped from Landsat in Central Europe. Remote Sens. Environ. 262, 112502.
Seidl, R., Turner, M.G., 2022. Post-disturbance reorganization of forest ecosystems in a changing world. Proc. Natl. Acad. Sci. U. S. A. 119.
Senf, C., Seidl, R., 2021. Mapping the forest disturbance regimes of Europe. Nat. Sustain. 4, 63–70.
Senf, C., Seidl, R., 2022. Post-disturbance canopy recovery and the resilience of Europe's forests. Glob. Ecol. Biogeogr. 31, 25–36.
Senf, C., Pflugmacher, D., Zhiqiang, Y., Sebald, J., Knorn, J., Neumann, M., Hostert, P., Seidl, R., 2018. Canopy mortality has doubled in Europe's temperate forests over the last three decades. Nat. Commun. 9, 4978.
Senf, C., Müller, J., Seidl, R., 2019. Post-disturbance recovery of forest cover and tree height differ with management in Central Europe. Landsc. Ecol. 34, 2837–2850.
Senf, C., Laštovička, J., Okujeni, A., Heurich, M., van der Linden, S., 2020. A generalized regression-based unmixing model for mapping forest cover fractions throughout three decades of Landsat data. Remote Sens. Environ. 240, 111691.
Senf, C., Sebald, J., Seidl, R., 2021. Increasing canopy mortality affects the future demographic structure of Europe's forests. One Earth 4, 749–755.
Smith-Tripp, S.M., Coops, N.C., Mulverhill, C., White, J.C., Axelson, J., 2024. Landsat assessment of variable spectral recovery linked to post-fire forest structure in dry sub-boreal forests. ISPRS J. Photogramm. Remote Sens. 208, 121–135.
Smola, A.J., Schölkopf, B., 2004. A tutorial on support vector regression. Stat. Comput. 14, 199–222.
Solans Vila, J.P., Barbosa, P., 2010. Post-fire vegetation regrowth detection in the Deiva Marina region (Liguria-Italy) using Landsat TM and ETM+ data. Ecol. Model. 221, 75–84.
Stevens-Rumann, C.S., Prichard, S.J., Whitman, E., Parisien, M.-A., Meddens, A.J.H., 2022. Considering regeneration failure in the context of changing climate and disturbance regimes in western North America. Can. J. For. Res. 52, 1281–1302.
Stiers, M., Willim, K., Seidel, D., Ammer, C., Kabal, M., Stillhard, J., Annighöfer, P., 2019. Analyzing spatial distribution patterns of European beech (*Fagus sylvatica* L.) regeneration in dependence of canopy openings. Forests 10, 637.
Strickland, M.K., Jenkins, M.A., Ma, Z., Murray, B.D., 2024. How has the concept of resilience been applied in research across forest regions? Front. Ecol. Environ. e2703 n/a.
Stritih, A., Bebi, P., Rossi, C., Grêt-Regamey, A., 2021a. Addressing disturbance risk to mountain forest ecosystem services. J. Environ. Manag. 296, 113188.
Stritih, A., Senf, C., Seidl, R., Grêt-Regamey, A., Bebi, P., 2021b. The impact of land-use legacies and recent management on natural disturbance susceptibility in mountain forests. For. Ecol. Manag. 484, 118950.
Stritih, A., Seidl, R., Senf, C., 2023. Alternative states in the structure of mountain forests across the Alps and the role of disturbance and recovery. Landsc. Ecol. 38, 933–947.
Stuart-Haëntjens, E.J., Curtis, P.S., Fahey, R.T., Vogel, C.S., Gough, C.M., 2015. Net primary production of a temperate deciduous forest exhibits a threshold response to increasing disturbance severity. Ecology 96, 2478–2487.
Trumbore, S., Brando, P., Hartmann, H., 2015. Forest health and global change. Science 349, 814–818.
Vandewiele, M., Geres, L., Lotz, A., Mandl, L., Richter, T., Seibold, S., Seidl, R., Senf, C., 2023. Mapping spatial microclimate patterns in mountain forests from LiDAR. Agric. For. Meteorol. 341, 109662.
Veraverbeke, S., Gitas, I., Katagis, T., Polychronaki, A., Somers, B., Goossens, R., 2013. Assessing post-fire vegetation recovery using red–near infrared vegetation indices: accounting for background and vegetation variability. ISPRS J. Photogramm. Remote Sens. 68, 28–39.
Viana-Soto, A., Okujeni, A., Pflugmacher, D., García, M., Aguado, I., Hostert, P., 2022. Quantifying post-fire shifts in woody-vegetation cover composition in Mediterranean pine forests using Landsat time series and regression-based unmixing. Remote Sens. Environ. 281, 113239.
Vieira, D.L.M., Scariot, A., 2006. Principles of natural regeneration of tropical dry forests for restoration. Restor. Ecol. 14.
White, J.C., Wulder, M.A., Hermosilla, T., Coops, N.C., Hobart, G.W., 2017. A nationwide annual characterization of 25 years of forest disturbance and recovery for Canada using Landsat time series. Remote Sens. Environ. 194, 303–321.
White, J.C., Saarinen, N., Kankare, V., Wulder, M.A., Hermosilla, T., Coops, N.C., Pickell, P.D., Holopainen, M., Hyyppä, J., Vastaranta, M., 2018. Confirmation of post-harvest spectral recovery from Landsat time series using measures of forest cover and height derived from airborne laser scanning data. Remote Sens. Environ. 216, 262–275.
White, J.C., Hermosilla, T., Wulder, M.A., Coops, N.C., 2022. Mapping, validating, and interpreting spatio-temporal trends in post-disturbance forest recovery. Remote Sens. Environ. 271.
White, J.C., Hermosilla, T., Wulder, M.A., 2023. Pre-fire measures of boreal forest structure and composition inform interpretation of post-fire spectral recovery rates. For. Ecol. Manag. 537, 120948.
Wulder, M.A., Roy, D.P., Radeloff, V.C., Loveland, T.R., Anderson, M.C., Johnson, D.M., Healey, S., Zhu, Z., Scambos, T.A., Pahlevan, N., Hansen, M., Gorelick, N., Crawford, C.J., Masek, J.G., Hermosilla, T., White, J.C., Belward, A.S., Schaaf, C., Woodcock, C.E., Huntington, J.L., Lymburner, L., Hostert, P., Gao, F., Lyapustin, A., Pekel, J.-F., Strobl, P., Cook, B.D., 2022. Fifty years of Landsat science and impacts. Remote Sens. Environ. 280, 113195.

Yan, L., Roy, D.P., Zhang, H., Li, J., Huang, H., 2016. An automated approach for sub-pixel registration of Landsat-8 operational land imager (OLI) and Sentinel-2 multi spectral instrument (MSI) imagery. Remote Sens. 8, 520.
Zehetgruber, B., Kobler, J., Dirnböck, T., Jandl, R., Seidl, R., Schindlbacher, A., 2017. Intensive ground vegetation growth mitigates the carbon loss after forest disturbance. Plant Soil 420, 239–252.
Zhu, Z., Woodcock, C.E., 2012. Object-based cloud and cloud shadow detection in Landsat imagery. Remote Sens. Environ. 118, 83–94.
Zhu, Z., Woodcock, C.E., 2014. Automated cloud, cloud shadow, and snow detection in multitemporal Landsat data: an algorithm designed specifically for monitoring land cover change. Remote Sens. Environ. 152, 217–234.